IEEE Access
Multidisciplinary | Rapid Review | Open Access Journal

Received August 1, 2021, accepted August 6, 2021, date of publication August 9, 2021, date of current version August 16, 2021.

Digital Object Identifier 10.1109/ACCESS.2021.3103824

Sustained Coordination of Devices in a Two-Layer Protection Scheme for DGs-Integrated Distribution Network Considering System Dynamics

EID ABDELBAKI GOUDA[1], ADEL AMER[2], AND AKRAM ELMITWALLY[1], (Member, IEEE)
[1]Department of Electrical Engineering, Faculty of Engineering, Mansoura University, Mansoura 35516, Egypt
[2]Siemens Energy Global GmbH & Co. KG, 111200 Munich, Germany

Corresponding author: Eid Abdelbaki Gouda (eaidgoda@mans.edu.eg)

ABSTRACT Distribution networks are usually protected by directional overcurrent relays (DOCRs). Besides, autoreclosers and fuses can be used for protecting lateral feeders to minimize power cuts. Coordinated operation of protection device must be maintained to ensure optimal fault isolation. Typically, steady-state fault current and static protective device characteristics are used to determine optimal settings of devices such that coordinated operation is verified. Sine fault current is not a steady signal and protection devices have dynamic behaviors, the conventionally-determined settings of devices can lead to loss of coordination jeopardizing system reliability. In this paper, a two-layer protection scheme is proposed for a distribution network with distributed generators (DGs). The first layer has DOCRs to protect main feeders. The second has autoreclosers and fuses to protect lateral feeders. Optimal settings of devices are determined to achieve both local-layer and inter-layer coordination of devices by constrained nonlinear optimization. Full dynamic models of every component and transient data of fault current are considered. Furthermore, to sustain coordination under DGs, a hybrid superconducting fault current limiter (HSFCL) with high temperature superconducting resistive element is connected in series to each DG. Dynamic modeling-based HSFCL cost minimization is searched by multi-objective optimization. The approach is applied to two distribution networks and simulation results are analyzed.

INDEX TERMS Overcurrent relay, fuse- recloser, transient, fault current limiter.

I. INTRODUCTION

Power distribution system is protected against abnormal events and faults that expose the system to severe high current [1]. The most common protective devices used in distribution system are overcurrent relays [2], [3]. Appropriate coordination between overcurrent relays should be maintained to guarantee simple, reliable, fast, and secure protection system [4]. Meanwhile, fuse-recloser combinations are widely employed protective arrangements when the rate of fault occurrence is high in lateral feeders [5]. During temporary faults, the recloser operates in fast-mode to clear the fault and recloses again after a preset time to prevent power cuts. The fuses do not operate in this case. But, if the fault is a permanent one, the fuse is melt after some interval to clear the fault. Then, the recloser slow-mode acts as backup protection for the fuse [6], [7]. So, a proper fuse-recloser coordination should be set to guarantee a reliable operation for the network and save the unnecessary fuse melting [6]–[8].

DG penetration in distribution system improves the reliability of the system, reduces voltage sag, and enhances the economics of the system [8]. Nonetheless, it can disturb protection system as current flow is no longer unidirectional and fault current magnitude changes. This can lead to undesired miscoordination between protection devices [7], [9]. Size, location, and type of DG, define its effect on the network protective scheme [10], [11].

Coordination between directional overcurrent relays (DOCRs) is obtained by selecting a pickup current (I_{pickup}), and a time dial setting (TDS) for each relay. The DOCR settings must ensure that a backup relay cannot work before a preset time interval from the supposed operation instant

The associate editor coordinating the review of this manuscript and approving it for publication was Nagesh Prabhu.

of the main relay for any fault. In this way, a fault is isolated with minimal amount of load power cuts. Several techniques were developed to solve the coordination problem such as curve fitting, graph theory, and optimization. Because there are many constraints in the problem, optimization is considered an effective method to find the settings of DOCRs [12]. Many optimization techniques are employed in the DOCR coordination problem [12]–[15]. In [13], mixed-integer linear programming is introduced to fit taking TDS as a discrete variable. Further, coordination problem related to fuse-recloser combination is studied in several papers. In [15], a two-stage technique is presented to assess the impact of DG penetration on the fuse-recloser combination. Firstly, the optimal locations of DGs are searched. Secondly, optimal recloser setting is determined to minimize the loss in coordination. Moreover, a microprocessor-based recloser is suggested for fuse saving at fault condition in [16].

Nowadays, fault current limiter (FCL) is viewed as a common solution for DG penetration drawbacks. Among many FCL technologies, magnetic, solid-state, and superconducting FCLs are usually utilized [17]. Authors in [18] and [19] used superconducting FCLs to overcome the impact of DGs penetration. Hence, the coordination of fuse-recloser combinations is restored by minimizing the DGs share in fault current. In [20] and [21], the DGs-related miscoordination between DOCRs is adjusted by connecting a FCL in series to each DG.

In most of published research like [13], [14], and [22], optimal coordination between protective devices consider only steady-state fault current. So, the operating time of each protection device is calculated by substituting the steady-state fault current value in a static current-time characteristics equation. This leads to approximated results and therefore inaccurate settings for relays. In practice, fault current has a dynamic transient behavior for a considerable time period before coming to a steady state. Thus, the transient behavior of fault current and FCL is studied in quite few works [23], [24]. The authors used the dynamic models to find the optimal settings of the relays to assure coordinated operation. However, the TDS only is optimized in [23] and [24]. The I_{pickup} setting is not optimized in the coordination algorithm that seriously degrades the quality of relay setting results.

FCL is proved to be an effective common solution to protection miscoordination problem caused by integration of various types of DG. Actually, FCL reduces the fault currents to levels close to the levels encountered before adding DGs. However, inappropriate small size of FCL will be insufficient to maintain coordination. Over-sized large FCL will unnecessarily enlarge the system cost. So, optimal sizes of FCLs must be identified [12]. Normally, most researchers do neglect the fault current transients and FCL dynamic behavior on setting protection devices and finding the optimal size of FCL. They replace the transient analysis by steady-state analysis which can lead to impractical decisions. For example, in [25], [26], the authors search for determining the optimal settings of DOCRs. But, they used the steady-state fault current to calculate the time of operation of each relay. They also use the steady-state characteristics curves for overcurrent relays instead of using its dynamic models. Moreover, DG transient behavior due to fault is not considered. DG model affects transient behavior of fault current and in turn the coordination of protective devices. So, the presumably optimal I_{pickup} and TDS settings reached with such simplifications caused relay miscoordination for some fault cases in the real-world system. Besides, in [12], [25], FCLs are used to mitigate the effect of DGs on the distribution system. But, FCL dynamic characteristics such as switching effect and performance delay time are not included. Discarding these dynamics leads to improper sizing of FCLs [27]. Also, fault currents may trip the circuit by relays prior to FCL operation. On the other side, fuse-recloser combination was realized to protect the distribution network in [27], [28]. Coordination between fuse and recloser under DGs is investigated.

However, in a real network, there can be different types of protection devices such as DOCRs and fuse-recloser combinations for protecting different zones in a wide distribution network. For this case, coordination between DOCRs, between fuse and recloser, between DOCR and recloser, and between fuses must be verified. In fact, protection coordination and maintenance of multi-layer protection system in DG-integrated networks is not searched in literature. Modeling, analysis tools, and solutions are yet unreported. For this reason, a new approach is proposed herein to coordinate operation of devices in a two-layer protection system for an active distribution system. Meanwhile, to get a robust and sustained coordination, dynamic behavior of all components is considered. In general, the previous works addressing the usage of FCLs to mitigate the impact of DGs on protection system has serious drawbacks as follows

1. They deal only with the relay-relay coordination or the recloser-fuse coordination. This lacks generality and practicality as the power system can have different types of protection devices and coordination between all devices should be sustained.
2. Calculation of operating times of protection devices use steady-state fault current and static characteristics of devices. This can lead to improper coordination and unreliable operation.
3. Dynamic models of DGs are neglected. Simplified static DG model is assumed.
4. Either synchronous or inverter-based DG is included.
5. Transient behavior of FCL is discarded.

In this paper, an effective two-layer protection system is proposed for a DGs-integrated distribution network. The first layer use DOCRs to protect the main feeders. The second layer uses fuse-recloser combinations to protect lateral feeders where higher rate of faults is expected. This structure of the protection system can lower the amount of tripped load and improves system resiliency. Basic optimal current and time settings are determined to minimize the protection system operation time and assure proper coordination between

main and backup devices. To better represent the practical operation of power system and enhance the protection system robustness, dynamic models of system components and DGs are used. Also, transient characteristics of fault currents are considered. To avoid the need for protection system resetting due to integration of a DG, FCLs are connected in series to the protection-disturbing DGs. An approach is proposed for optimal sizing of FCLs considering the dynamic behavior of all system components. This enables to obtain more accurate figures about the FCLs cost and ensure sustained coordination between protective devices in the two layers.

The contributions of this paper are:

1. A new two-layer design of the distribution network protection system is proposed. It improves the power network reliability, and minimizes power cuts.
2. The optimal device setting problem of this new protection system structure with four simultaneous coordination problem; DOCR-DOCR; DOCR-recloser; recloser-fuse; and fuse-fuse is studied for the first time.
3. Actual time-varying fault current signals are used instead of the steady-state rms values. Hence, the dynamic models of network elements, DGs, DOCRs, reclosers, and FCLs are integrated.
4. Hybrid superconducting FCLs are deployed to sustain protection coordination under integration of DGs. Optimal FCLs sizes are determined considering transient behavior of both fault current and FCL.
5. Impacts of both synchronous and inverter-based wind-turbine DGs are analyzed.

After this introduction, dynamic and static models of system components are described in Section II. Then, the proposed protection coordination method is analyzed in Section III. Next, the usage and sizing of FCLs for coordination maintenance is discussed in Section IV. Description and data of two case study systems come in Section V. Performance results are presented in Section VI. Finally, main conclusions are given in Section VII.

II. MODELS OF SYSTEM COMPONENTS

In this section, dynamic and static models of overcurrent relay, distributed generation, and FCL are presented.

A. DYNAMIC MODELS

1) OVERCURRENT RELAY

A dynamic model of DOCR is provided in IEEE standard C37.112-1996 as follows [29]:

$$S = \frac{1}{TDS}\int_{t=0}^{t=t_x}\frac{1}{f(I_{sc})}dt = 1 \tag{1}$$

For normal operation, the reset time $f(I_{sc})$ is defined as:

$$f(I_{sc}) = \frac{t_r}{1-\left(\frac{I_{sc}}{I_p}\right)^2} \tag{2}$$

For fault condition, the trip time $f(I_{sc})$ is defined as:

$$f(I_{sc}) = \frac{A}{\left(\frac{I_{sc}}{I_p}\right)^p - 1} + B \tag{3}$$

where, I_{sc} is the fault current, I_p is the pickup current. t_r, A, B, and p are constants that define the inverse type of overcurrent relay. For the chosen moderately inverse overcurrent relay characteristics, A is 0.0515, B is 0.114, and p is 0.02 [29]. The dynamic behavior of the relay depends on the ratio of fault current related to pickup current. t_x is the relay operation time.

2) DG MODEL

AC fault current produced by a DG of synchronous generator type has three states named as sub transient, transient, and steady-state [28]. Also, it has a DC component. So, the fault current is expressed as [23]:

$$I_{AC}(t) = \sqrt{2}E_g\left[\left(\frac{1}{X_d''}-\frac{1}{X_d'}\right)e^{\left(-\frac{t}{T_d''}\right)} + \left(\frac{1}{X_d'}-\frac{1}{X_d}\right)e^{\left(-\frac{t}{T_d'}\right)} + \left(\frac{1}{X_d}\right)\right]\sin(\omega t+\alpha) \tag{4}$$

$$I_{DC}(t) = \frac{E_g}{\sqrt{2}}\left[\left(\frac{1}{X_d''}+\frac{1}{X_q''}\right)e^{\left(-\frac{t}{T_a}\right)}\right]cos(\alpha) \tag{5}$$

Fig. 1 reveals the dynamic model of the wind-driven DG with doubly fed induction generator (DFIG). The model details are explained in [38]. The model parameters are given in Table 1.

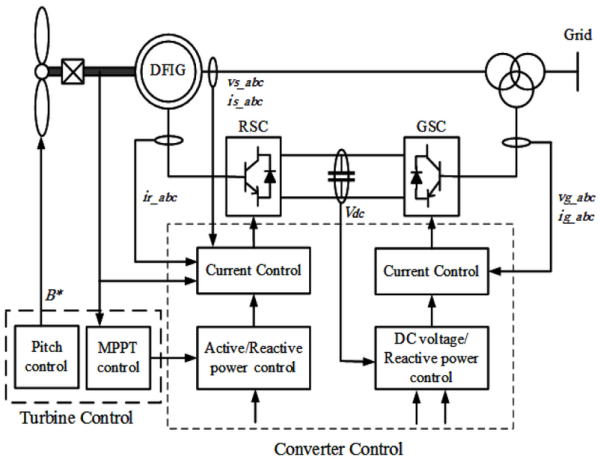

FIGURE 1. Model of wind-driven DFIG.

TABLE 1. Parameters OF DFIG model.

Parameter	Value
Cutoff frequency for the low pass filter	300 [Hz]
Main filter capacitance	300 [uF]
Damping branch capacitance	350 [uF]
Damping branch inductance	621 [uH]
Filter's damping resistance	1.332[ohm]
Voltage on the AC side of the grid-side converter	0.69 [kV]
Base DC voltage of DC bus	1.45 [kV]
Maximum current allowed in converter compared to nominal current at nominal voltage	1.2 [pu]
VSC reactor for grid-side Converter	192 [uH]
Maximum current allowed in converter compared to nominal current at nominal voltage	1.2 [pu]

Fault current produced by a wind-driven DG with doubly-fed induction generator (DFIG) is expressed as [38]:

$$\begin{aligned} \mathrm{I}(t) = V_s & \left[\left(\frac{1}{X_d''} - \frac{1}{X_d'} \right) e^{\left(-\frac{t}{T_d''} \right)} \right. \\ & \left. + \left(\frac{1}{X_d'} - \frac{1}{X_d} \right) e^{\left(-\frac{t}{T_d'} \right)} + \left(\frac{1}{X_d} \right) \right] \\ & \times \cos(\omega t - \alpha) - \frac{V_s}{2} \left[\left(\frac{1}{X_d''} + \frac{1}{X_q''} \right) \cos(\alpha) \right. \\ & \left. + \left(\frac{1}{X_d''} - \frac{1}{X_q''} \right) \cos(\omega t - \alpha) \right] e^{\left(-\frac{t}{T_a} \right)} \end{aligned} \quad (6)$$

where, X_d, X_d', X_d'' is the d-axis synchronous, transient, and sub-transient reactance; X_d'' is the q-axis sub-transient reactance; T_d', T_d'' are the transient and sub-transient time constants; T_d is the armature time constant, E_g is the internal voltage of the generator, V_s is stator voltage, α is the phase angle of the short circuit current at fault instant.

3) FCL MODEL

In this paper, FCL is applied as a solution to mitigate the negative impact of DGs. Specifically, hybrid superconducting fault current limiter (HSFCL) with high temperature superconducting (HTSC) element is used [30]. HSFCL consists of the current limiting element, fast switch, and HTSC element as shown in Fig. 2. The fast switch consists of short bar (SB) switch, vacuum interrupter (VI), driving coil, and electromagnetic (EM) repulsion plate. The current limiting part contains the breaking switch and the current limiting resistance (CLR). In normal operation, the repulsion plate VI and breaking switch are closed while SB is open. During fault, SB closes through a control circuit as the bypassed quench current flows into the driving coil from the HTSC element when the current exceeds a setting value. To keep the current flowing in the driving coil until it reaches a pre-set value, VI stays in a close position. Then, the repulsion plate VI and the breaking switch open, which leads to the fault current limiting by the CLR element. The SFCL dynamic model is mathematically

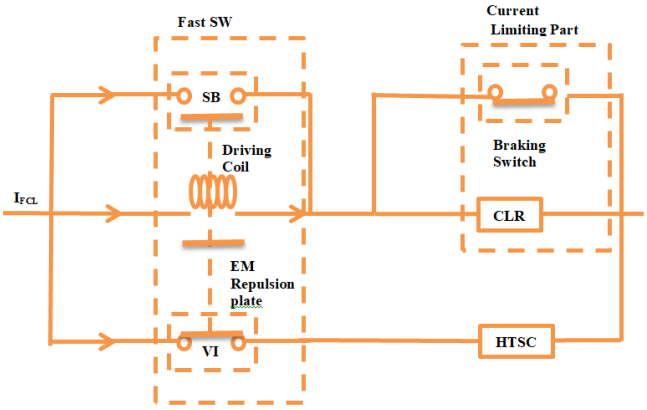

FIGURE 2. Main components of HSFCL.

expressed as follows [35]:

$$R_{SFCL}(t) = R_n \left[1 - exp\left(\frac{t - t0}{Tf} \right) \right]^{\frac{1}{2}} \quad t0 < t < t1 \quad (7)$$

$$R_{SFCL}(t) = a(t - t1) + R_r \quad t1 < t < t2 \quad (8)$$

$$R_{SFCL}(t) = b(t - t2) + R_{r1} \quad t > t2 \quad (9)$$

Equation (7) shows the resistance value change of the HTSC element when the quench happens. Equations (8) and (9) show the recovery resistance of the HTSC element. The HTSC recovers again to its superconducting phase through two stages. Firstly, it recovers slowly for certain milliseconds and after that in the second stage it recovers quickly to superconducting state [35].

Where in (7)-(9), R_n, Tf and t0 are the convergence resistance, time constant and quench starting time, respectively. R_r, a, t1 are the recovery starting resistance, the initial recovery slope and the recovery starting time, respectively. R_{r1}, b, and t2 are the second stage recovery starting resistance, the recovery slope and the recovery starting time, respectively.

B. STATIC CHARACTERISTICS

1) CHARACTERISTICS OF DOCR

The characteristics of the DOCR are described as [12]:

$$t_i = TDS_i \left(\frac{A}{M_i^C - 1} + B \right) \quad \text{with} \quad M_i = \frac{I_{fi}}{I_{pi}} \quad (10)$$

$$t_{j,i} = TDS_{j,i} \left(\frac{A}{M_{j,i}^C - 1} + B \right) \quad \text{with} \quad M_{j,i} = \frac{I_{fj,i}}{I_{pi}} \quad (11)$$

where, t_i is the operating time of the i^{th} DOCR regarding to fault at i, $t_{j,i}$ is the operating time of the j^{th} DOCR regarding to fault at i, TDS_i is the time dial setting of relay i, $TDS_{j,i}$ is the time dial setting of relay j, I_{fi} is the short circuit current seen by relay i, $I_{fj,i}$ is the short circuit current seen by relay j for fault at relay i, and A, B, C are constants that define the relay characteristics. For the moderately inverse overcurrent relay characteristics, A = 0.0515, B = 0.114, and C = 0.02 [26].

2) FUSE-RECLOSER COMBINATION

Fuse-recloser combination is a common strategy to protect distribution systems. Recloser has a fast mode that operates during temporary faults to clear this kind of fault before the fuse is melt. Otherwise, if the fault is permanent, the fuse isolates the fault. Recloser has a slow mode that would work as backup protection for the fuse when it fails to clear the fault.

Mathematically, the characteristics of the recloser are [13]:

$$t_{ir} = TDS_{ir}\left(\frac{A_r}{\left(\frac{\mathrm{I_{fri}}}{PCS_r}\right)^{C_r} - 1} + B_r\right) \tag{12}$$

$$\mathrm{PCS_r} = \mathrm{OLF\ x\ Ilmax} \tag{13}$$

where, for the i^{th} recloser, t_{ir} is the operating time; TDS_{ir} is the time dial setting; I_{fri} is the short circuit current seen by the recloser. The constants A_r, B_r, C_r define the recloser type. OLF is the overload factor, and *Ilmax* is the maximum value of the load current passing through the recloser.

Also, characteristics of a fuse are expressed as [13]:

$$\log(t) = a\log(I) + b \tag{14}$$

where, t and I are the associated operating time and current. The coefficients a and b depend on fuse type.

III. PROPOSED PROTECTION COORDINATION METHOD

The actual transient fault current must be used instead of the steady-state rms fault current to estimate the true operating time of relays as discussed in [24]. Therefore, fault current should be time-sampled to represent the fault current dynamics.

A. DETERMINATION OF RELAY OPERATING TIME

The proposed method is based on dividing the time-varying fault current magnitude signal into a number of segments (h) as shown in Fig. 3. The average value of fault current in these segments are $I1, I2, \ldots.$, and Ih, respectively. The operating time of each relay can be calculated as follows [24]:

$$\int_{t_0}^{t_1} \frac{\mathrm{d}t}{\mathrm{M_1} * \mathrm{TDS}} + \int_{t_1}^{t_2} \frac{\mathrm{d}t}{\mathrm{M_2} * \mathrm{TDS}} + \cdots + \int_{t_{h-1}}^{t_x} \frac{\mathrm{d}t}{\mathrm{M_h} * \mathrm{TDS}} = 1 \tag{15}$$

$$\mathrm{M}_j = \frac{A}{\left(\frac{I_j}{I_{pickup}}\right)^p - 1} + B \tag{16}$$

where, I_j is the average fault current magnitude in the j^{th} segment as shown in Fig. 3.

Equation (15) is rewritten as:

$$\frac{t_1 - t_0}{\mathrm{M_1}} + \frac{t_2 - t_1}{\mathrm{M_2}} + \cdots + \frac{t_x - t_{h-1}}{\mathrm{M_h}} = \mathrm{TDS} \tag{17}$$

The operating time of the relay (t_x) is got from (17) as:

$$t_x = \mathrm{M_h} * \mathrm{TDS} + \sum_{i=1}^{h-1} t_i \left(\frac{\mathrm{M_h}}{\mathrm{M}_{i+1}} - \frac{\mathrm{M_h}}{\mathrm{M}_i}\right) + t_0 \left(\frac{\mathrm{M_h}}{\mathrm{M_1}}\right) \tag{18}$$

t_0 is the fault detection time. Denoting the second and third terms in the R. H. S. of (18) by b, the operating time of the main relay (t_m) and of the backup relay (t_b) are obtained as [24]:

$$\mathrm{t_m} = \mathrm{M_{hm}} * \mathrm{TDS_m} + \mathrm{b_m} \tag{19}$$

$$\mathrm{t_b} = \mathrm{M_{hb}} * \mathrm{TDS_b} + \mathrm{b_b} \tag{20}$$

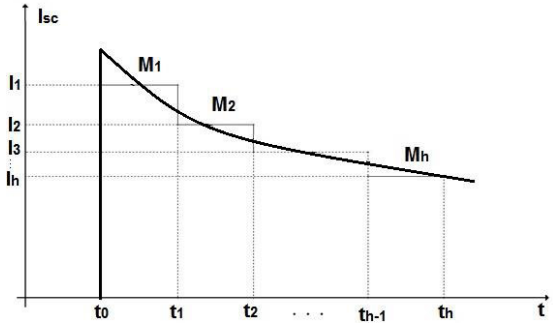

FIGURE 3. Fault current magnitude signal sectionalized.

B. OPTIMAL SETTING PROBLEM

The two-layer protection system of the distribution network has DOCRs in the first layer for protecting the system against faults on the main feeders. It also has fuse-recloser combinations in the second layer to protect the system against faults on lateral feeders. The DOCRs work also as backup protection to the fuse-recloser combinations. Proper coordination between the DOCRs, between the recloser and fuses, between a fuse and another fuse, and between the DOCRs and the reclosers must be designed to ensure fast and reliable operation of the system. Coordination of protective devices is achieved by selecting the optimal settings of each. The coordination problem is formulated as a constrained nonlinear optimization problem. The objective is to find the minimum sum of operating times of all protective devices to provide fast clearance of faults. So, the objective function (F) is proposed as follows:

$$min\ F = \sum_{i=1}^{H} t_{OC,i} + \sum_{g=1}^{Q} \sum_{n=1}^{M} \left(t_{Rg,fm,n} + t_{Rg,sm,n} + \sum_{k=1}^{L_n} t_{F,nk}\right) \tag{21}$$

The fuse and recloser (second layer) coordination constraints are [28]:

$$t_{F,nk} - t_{R,fm,n} > \frac{\mathrm{MRCTI}}{2} \tag{22}$$

$$t_{F,n(k+1)} - t_{F,nk} > \mathrm{MFCTI} \tag{23}$$

$$t_{R,sm,n} - t_{F,nk} > \frac{\mathrm{MRCTI}}{2} \tag{24}$$

$$t_{R,sm,n} - t_{R,fm,n} > \mathrm{MRCTI} \tag{25}$$

The relay-recloser (two-layer interface) coordination constraint is:

$$t_{OC,n,backup} - t_{R,sm,n} > \mathrm{MRCTI} \tag{26}$$

The relay-relay (first layer) coordination constraints are [12]:

$$t_{OC,backup} - t_{OC,main} > \text{CTI} \tag{27}$$

Setting parameter limit constraints are [12], [28]:

$$TDS_{min} \leq TDS_{fm} \leq TDS_{\max} \tag{28}$$
$$TDS_{min} \leq TDS_{sm} \leq TDS_{\max} \tag{29}$$
$$TDS_{min} \leq TDS_{OCi} \leq TDS_{\max} \tag{30}$$
$$\mathrm{I_{p,\,min}} \leq \mathrm{I_{pi}} \leq \mathrm{I_{p,max}} \tag{31}$$
$$\mathrm{a_{k,\,min}} \leq a_k \leq \mathrm{a_{k,max}} \tag{32}$$
$$\mathrm{b_{k,\,min}} \leq \mathrm{b_k} \leq \mathrm{b_{k,max}} \tag{33}$$

where $t_{OC,i}$ is the i^{th} DOCR operating time; H is the total number of DOCRs; $t_{Rp,fm}$ and $t_{Rp,sm}$ are the operating time for the fast and slow modes of the g^{th} recloser, respectively. Q is the total number of reclosers. $t_{F,nk}$ is the operating time of the k^{th} fuse for a fault at node n. M is the number of nodes protected by the g^{th} recloser. L_n is the number of fuses between the fault point (n) and a recloser. MRCTI, MFCTI, and CTI are the minimum coordination time interval for the recloser, fuse, and DOCR, respectively. TDS_{min}, TDS_{max} are the minimum and maximum time dial setting, respectively. $\mathrm{TDS_{fm}}$ and $\mathrm{TDS_{sm}}$ are the recloser fast and slow mode values for TDS. $\mathrm{I_{p,\,min}}$ and $\mathrm{I_{p,max}}$ are the minimum and maximum pickup current setting, respectively, $\mathrm{a_{k,min}}$, $\mathrm{a_{k,min}}$, $\mathrm{b_{k,max}}$, $\mathrm{b_{k,max}}$ are the minimum and maximum values for fuse characteristics coefficients.

IV. RESTORING PROTECTION COORDINATION BY FCLS

Integration of DGs changes fault current substantially. So, they can cause miscoordination of earlier-set protection devices [12], [18]. FCLs are suggested in literature as an efficient solution to maintain protection coordination under DGs [18], [19]. FCLs can be inserted in any branch in the system but connected in series to each DG is proved to be the most practical [35]. Nonetheless, their optimal sizes, series impedance values, must be determined. Neglecting the dynamics of system components and fault transients, a multi-objective optimization-based method is presented in [12] to optimally size the FCLs. Multi-objective particle swarm optimization (MOPSO) technique is employed to solve the optimization problem and find the optimal FCL impedance [36]. However, there can still some miscoordinated devices after the use of FCLs because system dynamics are neglected on determining the FCL size. So, the FCLs sized by [12] cannot be adequate to restore full coordination of devices considering actual system dynamics.

To identify the adequate size of the HSFCLs CLR resistance vector (**R**), a technique is proposed in this work as follows:

1. Neglecting system dynamics, use the method reported in [12] to find the preliminary optimal HSFCLs resistance vector (Rs).
2. Use Rs as an initial value for R.
3. Construct the dynamic model of the network, DGs and HSFCLs in PSCAD.
4. Apply R to the system model.
5. Run the dynamic system model to get the time-domain current signals for three-phase local fault seen by each protective device. Save the fault current signals in a matrix (IF).
6. Transfer (IF) to Matlab environment where the protection coordination algorithm discussed in Section 3 is coded.
7. Compute the operating times of each main and backup device. Then, check all coordination constraints in (22)-(33).
8. If any miscoordination exists, increase R by 5
9. Save results.

Fig. 4 demonstrates a schematic diagram for the dynamic HSFCL sizing technique.

V. CASE STUDY SYSTEMS

Traditionally, fault current is obtained as a single-valued phasor having a magnitude and a phase angle. Typically, fault current calculation algorithm uses the network line impedance matrix and the pre-fault bus voltage phasor to compute the fault current phasor. Actually, the fault current is a dynamic signal that has a considerable non-sinusoidal transient behavior before reaching an approximate steady-state pattern, as in (4) and (5). These transients can be notable for about 0.2 s from fault instant [24]. So, neglecting the fault current transients and considering only the steady-state rms value of fault current in setting the protective devices may lead to mal-operation and protection miscoordination [25]. Moreover, in time-domain simulation studies, to get accurate

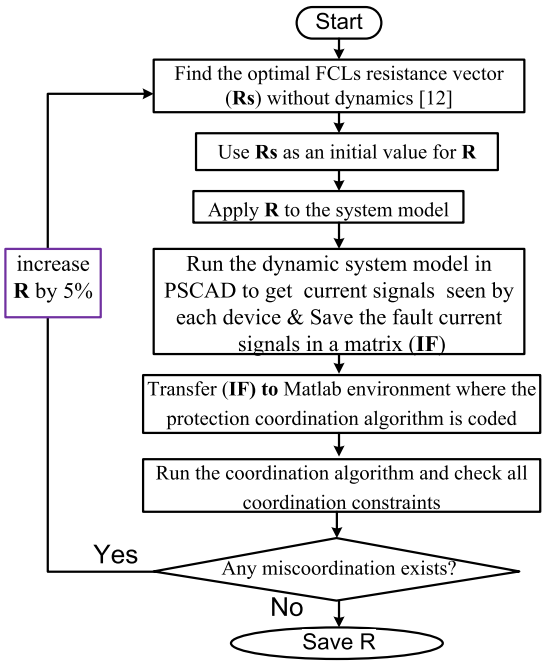

FIGURE 4. Flowchart for FCLs sizing with dynamic limiter model.

fault current signals, the time-domain dynamic models of network branches, synchronous generators, DGs, and FCL must be integrated. The whole network is time-domain simulated under fault, using a time-domain simulator like PSCAD, to obtain the fault current signal. To cater a time-varying fault current signal, a protective device must have a dynamic model that can interact with the time variation of the fault current signal instead of the conventional phasor-based models [29].

The proposed approach is applied to two test systems. The first is the IEEE 33-bus radial system as a typical distribution system [31]. The second is the 33kV distribution part of the IEEE 30-bus meshed systems with detailed data in [32]. As shown in Fig. 5, the IEEE 33-bus system is protected by 17 DOCRs (R1-R17) that represent the first protection layer assigned to protect the main lines. There are also 3 reclosers, and 12 fuses that form the second protection layer hired to protect the lateral feeders. It includes the lateral feeder leaving bus 2 that is protected by recloser Rc1 and 3 fuses (F1 to F3); the lateral feeder leaving bus 3 that is protected by recloser Rc2 and 2 fuses (F4, F5); and the lateral feeder leaving bus 6 that is protected by recloser Rc3 and 7 fuses (F6 to F12).

The studied part of the IEEE 30-bus system is revealed in Fig. 6. It is protected by 29 DOCRs (R1-R29) in the first layer and 6 fuses (F1-F6) with 3 reclosers (Rc16, Rc17 and Rc30) in the second layer. The fuses F1, F2 are located on the lateral feeder supplying loads at bus 16. These fuses must be coordinated with recloser Rc16. The fuses F3, F4 are located on the lateral feeder supplying loads at bus 17. These fuses must be coordinated with recloser Rc17. The fuses F5, F6 are located on the lateral feeder supplying loads at bus 30. These fuses must be coordinated with recloser Rc30. The dynamic models of both systems in Figs. 5 and 6 are implemented in PSCAD/EMTDC. Besides, the protection devices setting problem formulated in subsection III.B is coded in Matlab. One m-file is made for the case when realistic dynamic models of protective devices are used. Another m-file is prepared for the case when approximate static models are used. Particle swarm optimization (PSO) is used to solve the optimization problem [33]. First, local fault current seen by

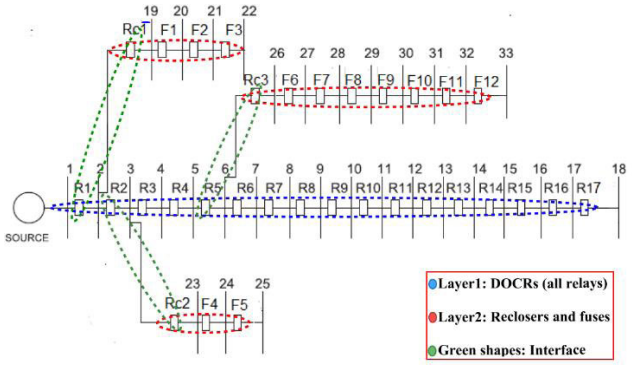

FIGURE 5. IEEE 33 bus system.

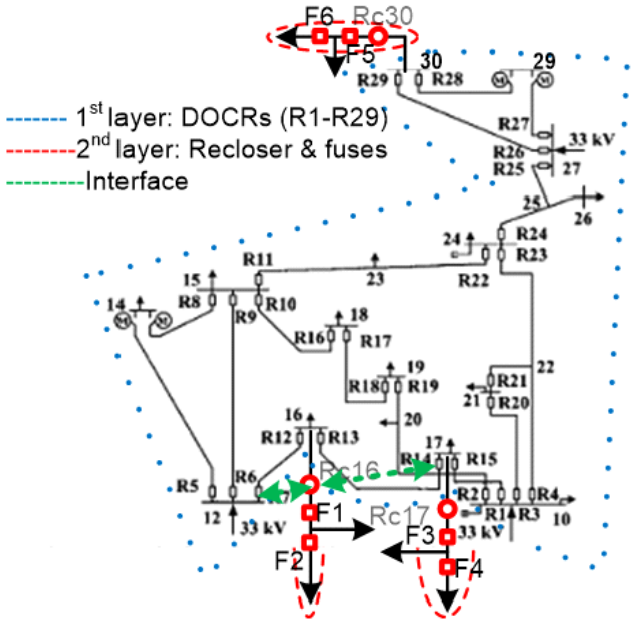

FIGURE 6. Part of IEEE 30-bus meshed system.

every protective device is simulated in PSCAD. It is obtained as a sampled time-domain string and saved as a row in a matrix called (MI). Meanwhile, the sampled time-domain fault current(s) seen by its backup device(s) is obtained and saved as row(s) in another matrix called (BI). The number of MI/BI columns is the number of samples in the fault current (600 samples for 15 cycles). Then, matrices MI and BI are transferred to Matlab environment for further processing. The coordination indices are taken as CTI = 0.2 s, MRCTI = 0.5 s, and MFCTI = 0.5 s [13], [24]. Resistive HSFCLs with the parameters shown in Table 2 are assumed.

VI. PERFORMANCE RESULTS

A. RESULTS OF THE IEEE 33-BUS SYSTEM

1) OPTIMAL SETTING

First, the optimal setting problem discussed in subsection III.B is solved by particle swarm optimization (PSO) with parameters stated in Table 3 [33]. The obtained optimal settings of the DOCRs, reclosers and fuses using steady state fault currents and static models of devices (no dynamics case) are indicated by blue solid circles in Figs. 7, 8 and 9. Also, fault current dynamics and devices dynamic time-current models are considered. The got settings of devices are indicated by black squares in Figs. 7, 8 and 9.

Actually, the settings got in the no dynamics-case satisfy all the coordination constraints for steady-state fault current. However, coordination may be lost if the real fault current dynamics are considered. To verify, dynamic protective device characteristics and time-domain fault current signals are used. Operating times of devices are calculated as described in subsection III.A.

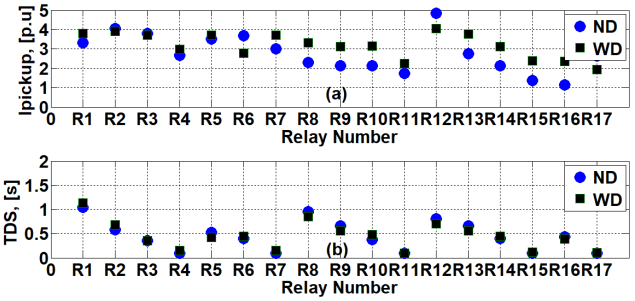

FIGURE 7. Setting of DOCRs of IEEE 33 bus system without dynamics (ND) and with dynamics (WD), (a) current, (b)time.

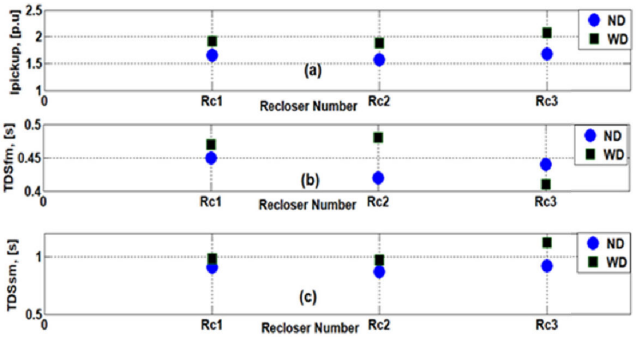

FIGURE 8. Setting of reclosers of IEEE 33 bus system without dynamics (ND) and with dynamics (WD), (a) current, (b)fast mode time, (c) slow mode.

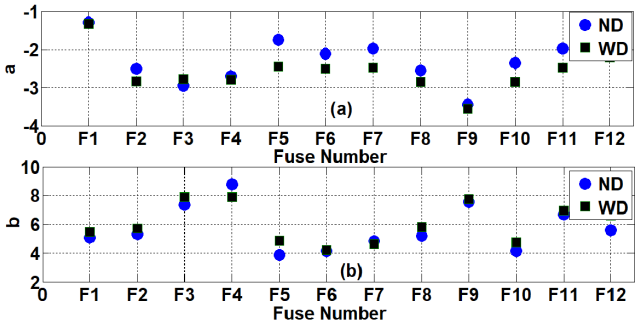

FIGURE 9. Setting of fuses of IEEE 33 bus system without dynamics (ND) and with dynamics (WD), (a) a, (b) b.

TABLE 2. HSFCL modelling parameters.

Material	YBCO
Manufactured form	Thin film
Critical temperature	87K
Tf	0.01
a1	-20
a2	-50
b1	5
b2	3

TABLE 3. PSO parameters.

Pop. size	max iterations	c1 & c2	Wmax	Wmin
30	2000	2	0.9	0.4

TABLE 4. Operating time difference between protection devices with different scenarios for ieee 33-bus radial system.

main-backup devices	operating time difference, s					
	NGND	NGWD	IGWD	SGWD	SGWDSL	SGWDDL
R1BR2	0.28	0.71	0.64	3.65	0.27	0.21
R2BR3	0.3	0.47	0.72	0.32	0.27	0.58
R3BR4	0.3	0.46	0.53	0.3	0.28	0.58
R4BR5	0.32	0.72	0.25	0.62	1.12	0.82
R5BR6	0.47	0.42	0.38	0.86	0.73	0.7
R7BR8	0.28	0.37	0.42	0.79	1.19	1.92
R8BR9	0.76	0.36	-0.74	0.33	0.25	0.29
R9BR10	0.18	0.38	0.25	0.16	0.32	0.62
R10BR11	0.28	0.41	0.24	0.38	0.3	0.86
R11BR12	0.26	0.33	0.26	0.41	1.76	0.32
R12BR13	0.15	0.36	1.01	1.65	0.27	0.3
R13BR14	0.27	0.22	0.64	0.12	0.41	0.62
R14BR15	0.28	0.23	0.47	0.61	0.3	0.25
R15BR16	0.76	0.64	0.6	0.54	1.02	0.71
R16BR17	0.3	0.87	1.55	0.41	0.24	0.3
F1BRc1fm	2.15	0.29	0.35	0.87	-0.72	1.76
F2BRc1fm	0.92	0.64	0.9	0.05	0.21	0.27
F3BRc1fm	0.28	1.22	0.68	0.66	0.34	0.41
Rc1smBF1	0.52	0.93	0.41	0.61	0.48	0.52
Rc1smBF2	0.3	0.64	0.51	0.54	0.51	0.65
Rc1smBF3	0.16	0.72	0.22	0.48	0.59	0.27
F1BF2	0.51	0.53	0.41	-1.1	0.54	0.54
F2BF3	0.62	0.56	0.81	1.36	0.99	0.65
F4BF5	0.54	0.98	0.87	0.4	0.4	0.85
F6BF7	0.92	0.71	0.41	0.5	0.52	0.61
Rc1smBRc1fm	0.74	0.57	0.61	-2.29	0.01	1.02
R1BRc1sm	0.65	0.58	0.66	0.71	0.77	0.89
F4BRc2fm	0.51	1.49	0.55	3.4	1.32	0.41
F5BRc2fm	0.71	0.57	0.6	0.65	0.79	0.27
Rc2smBF4	0.65	2.19	1.55	0.78	1.87	0.54
Rc2smBF5	0.14	0.47	0.25	0.42	0.28	0.26
Rc2smBRc2fm	0.36	0.6	0.25	0.36	0.25	0.79
R2BRc2sm	0.55	0.66	0.88	0.9	0.87	0.76
F6BRc3fm	0.66	1.55	0.27	0.41	0.51	0.48
F7BRc3fm	0.41	0.35	0.22	0.62	0.59	0.62
F8BRc3fm	0.57	0.9	0.32	0.18	0.79	0.7
F9BRc3fm	1.49	0.68	0.41	0.65	0.35	0.62
F10BRc3fm	0.57	0.78	0.51	0.78	0.71	0.7
F11BRc3fm	1.43	1.9	0.27	0.81	0.41	0.28
F12BRc3fm	0.3	0.78	2.01	0.87	0.62	0.68
Rc3smBF6	0.14	0.78	2.02	0.41	0.58	0.43
Rc3smBF7	0.5	0.68	0.28	0.21	0.57	0.86
Rc3smBF8	0.28	0.62	0.27	0.22	0.69	0.81
Rc3smBF9	0.91	0.58	-3.48	0.51	1.88	0.38
Rc3smBF10	0.9	0.68	0.77	0.74	0.41	0.63
Rc3smBF11	0.54	0.38	1.14	0.29	0.62	0.28
Rc3smBF12	1.25	0.64	0.28	0.28	0.71	0.68
Rc3smBRc3fm	0.5	0.72	1.12	0.25	0.57	0.83
R5BRc3sm	0.66	0.99	1.11	1.34	1.12	1.62
F7BF8	0.58	0.66	0.72	0.31	1.49	0.57
F8BF9	0.62	0.78	0.52	0.74	0.57	0.69
F9BF10	0.68	0.66	0.91	0.51	1.19	0.88
F10BF11	0.87	0.72	0.51	0.78	0.47	0.57
F11BF12	0.54	0.67	0.77	0.64	0.6	0.79
No. of miscoordinations	5	0	5	12	5	0

Thus, difference of operating time between each main-backup device pair is assessed and set in Table 4. The results of 6 scenarios are exhibited in Table 4. The first scenario is no DG- no dynamics-based settings (NGND) in the second column; the second scenario is no DG- with dynamics-based settings (NGWD) in the third column; the third scenario is under inverter-based DG- with dynamics-based settings (IGWD) in the fourth column; the fourth

scenario is under synchronous DG- with dynamics-based settings (SGWD) in the fifth column; the fifth scenario is under synchronous DG- with dynamics-based settings and statistic FCL model (SGWDSL) in the sixth column; the sixth scenario is under synchronous DG- with dynamics-based settings and dynamic FCL model (SGWDDL) in the seventh column. In Table 4, the letter 'B' precedes the backup device. It is noted that 5 miscoordination cases occur between main-backup protection devices as highlighted in Table 4 for the NGND scenario. As can be observed in the 3rd column of Table 4, all miscoordination cases disappear for the NGWD scenario. Fig. 10 shows the static time-current characteristics (TCC) of reclosers and fuses. It models the fuses accurately but it represents the recloser approximately. The dynamic characteristics of recloser cannot be represented by TCC.

2) EFFECT OF DGS

Two synchronous generator-based DGs are installed at bus 5 and bus 2. Each DG has a power rating of 90 kVA and a 0.2 p.u sub-transient reactance. Considering fault current and protective device dynamics, the operating time of each device is determined using the dynamics-based settings obtained in Figs. 7, 8 and 9. The difference of operating time between the related main-backup devices is provided in Table 4. It is noted that 12 miscoordinated items occur for this SGWD scenario. Moreover, to evaluate the impact of DG type, two 90 kVA inverter-based DFIG DGs substitute the synchronous DGs [34]. This matches the IGWD scenario in Table 4. Fig. 11 illustrates fault current signals before and after adding DGs.

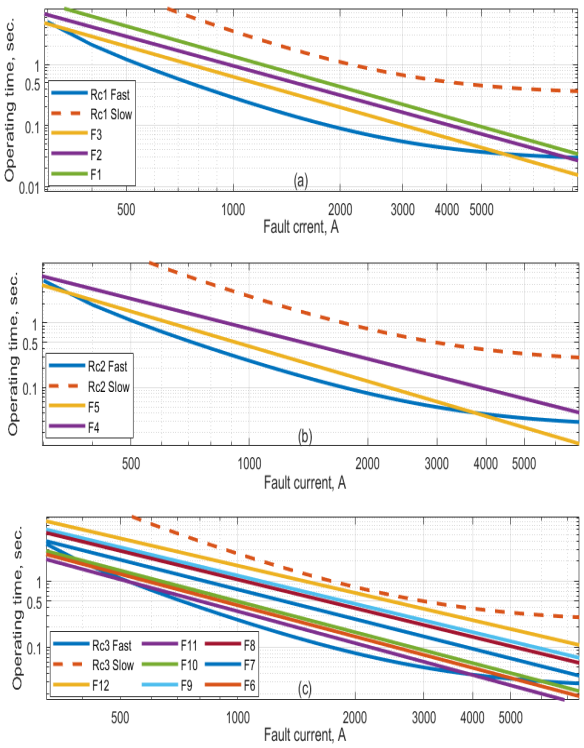

FIGURE 10. Static characteristics for reclosers and fuses, (a) Rc1, F1, F2, F3, (b) Rc2, F4, F5, and (c) Rc3, F6, F7, F8, F9, F10, F11, F12.

It is inferred from Fig. 11 that connection of inverter-based DGs moderately affects the fault current signals. Whereas, the synchronous DG largely varies the fault current signals causing more miscoordination in the protection system as observed in Table 4.

3) HSFCL SIZES

Table 5 gives the attained optimal resistance values of FCLs neglecting current and FCL dynamics using [12]. Fig. 12 shows the steady state fault currents seen by devices before DGs, after DGs and after adding the FCLs given in the second column of Table 5.

It is evident from Fig. 12 that integrating FCLs in series to the DGs reduces the fault current magnitude to be close to its levels before connecting DGs in the distribution system. This implies that the protection miscoordination is mitigated by FCLs. However, there can still some miscoordinated devices because system dynamics are neglected on determining the FCL size in Table 5. So, the above FCL size cannot be adequate to restore full coordination of devices considering actual system dynamics.

TABLE 5. Location and sizes of FCLs.

Location	Resistance, p.u	
	Neglecting all dynamics	Considering all dynamics
DG at Bus 5	3.01	4.92
DG at Bus 21	3.71	7.21
Summation of FCLs sizes	6.72	12.13
Total FCLs cost	1.78M$	2.59 M$

To examine the coordination of related main-backup protection devices, Table 4 compares the differences of operating time of main-backup device pairs for the SGWD and SGWDSL scenarios. As remarked, 5 miscoordination cases still exists after the use of the ideal FCLs sited in Table 5. The remaining loss of protection coordination is due to ignoring HSFCL dynamics which influences the fault current transients. Eventually, this leads to inadequate sizing of the FCL resistance. Table 5 presents the updated HSFCL resistance values obtained by the proposed method in Section IV. They assure full coordination of protective devices considering dynamic models of all components as manifested in 7th column of Table 4 (SGWDDL scenario). Interestingly, including the dynamic behavior of HSFCLs caused an increase in the FCL size by about 60% and in the FCL cost by about 30%.

B. RESULTS OF THE IEEE 30-BUS SYSTEM

1) OPTIMAL SETTING

First, using the steady state fault current and the static characteristics of protective devices, the optimal setting problem discussed in subsection III.B is solved by PSO with the parameters stated in Table 3. Figs. 13–15 show the obtained

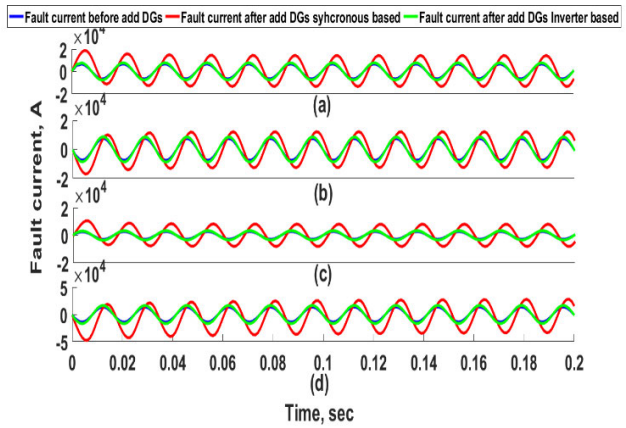

FIGURE 11. Fault current signals before and after adding DGs (a) Relay 4, (b) Relay 6, (c) Fuse3, (d) Recloser Rc2.

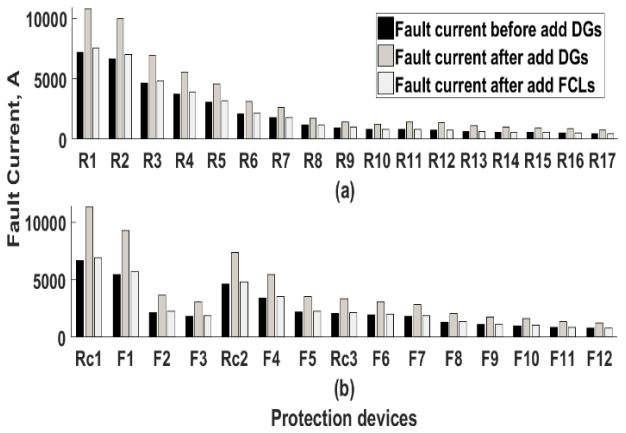

FIGURE 12. Steady-state fault current levels before DGs, after DGs, and after static FCLs.

optimal settings of the protective devices using steady-state fault currents (no dynamics) illustrated by the blue dots. Besides, the same protection devices setting problem is solved again when the fault current dynamics are considered (with dynamics). The corresponding settings are represented by the black squares in Figs. 13–15.

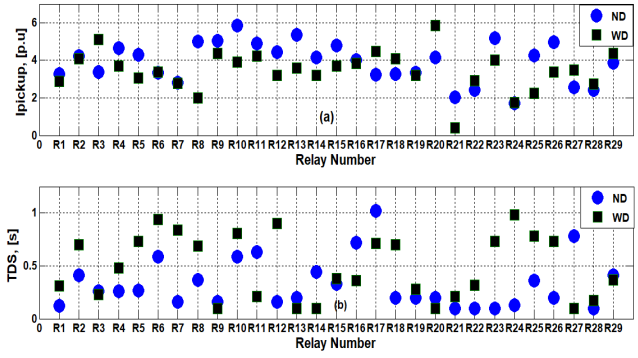

FIGURE 13. Setting of DOCRs IEEE 30 bus System without dynamics (ND) and with dynamics (WD), (a) current, (b)time.

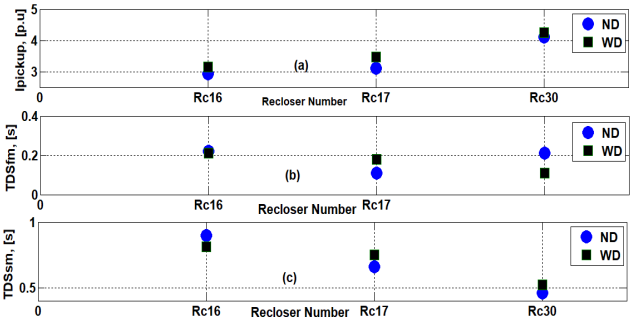

FIGURE 14. Setting of reclosers of IEEE 30 bus system without dynamics (ND) and with dynamics (WD), (a) current, (b) fast mode time, (c) slow mode time.

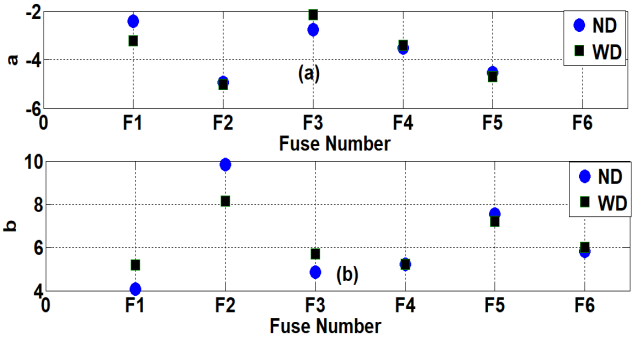

FIGURE 15. Setting of fuses of IEEE 30 bus system without dynamics (ND) and with dynamics (WD), (a) a, (b) b.

Basically, the got no-dynamics settings satisfy all the coordination constraints under steady-state fault current. However, coordination may be lost if the real fault current dynamics are used to compute the device operating time. To confirm, the power system is time-domain simulated in PSCAD to get the fault current signals. Using the no dynamics-based protective device settings and full fault current signals, operating times of devices are calculated as described in subsection III.A. Thus, different coordination constraints are assessed and presented in the third column of Table 6 (NGWD scenario). In analogy to Table 4, 6 scenarios are also presented in Table 6. It is noted that 24 miscoordination cases occur for NGND scenario while zero miscoordination cases occur for NGWD scenario.

2) EFFECT OF DGS

Three synchronous generator-based DGs are installed at bus 10, 12 and 19, respectively. Each DG has a rating of 50MW, a unity power factor, and a sub-transient reactance of 0.2 p.u. Considering fault current and protective device dynamics, the operating time of each device is determined using the dynamic-based settings obtained in Figs. 13–15. The difference of operating time between the related main and backup devices is provided in Table 6 (SGWD scenario). Moreover, to evaluate the impact of DG type, three 50MW DFIG as inverter-based DGs replace the previous synchronous DGs. This forms the IGWD scenario in Table 6. Fig. 16 depicts

samples of fault current signals before and after adding DGs in IEEE 30 bus system. It is marked that adding inverter-based DGs moderately affects the fault current signals. Whereas, the synchronous DG largely varies the fault current signals that leads to more miscoordination in the protection system as observed in Table 6.

3) HSFCL SIZES

Table 7 gives the obtained optimal resistance values of FCLs when system dynamics are neglected using the method in [12]. Fig. 17 shows samples of fault current signals seen by protective devices before DGs, after synchronous DGs and after adding the FCLs sized in Table 7.

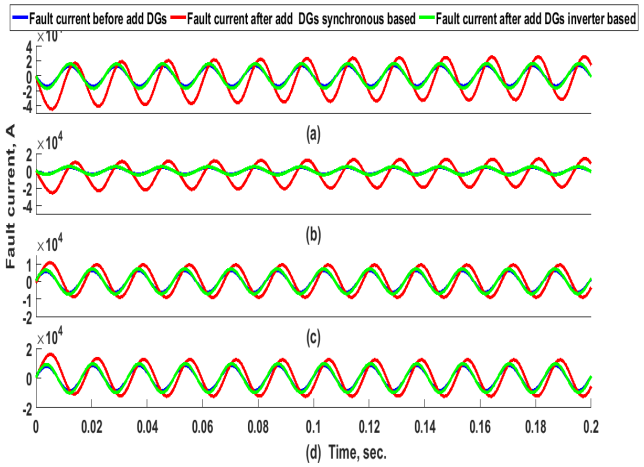

FIGURE 16. Fault current signals before and after adding DGs (a) Relay 3, (b) Relay 18, (c) Relay 24, (d) Fuse2.

It is evident from Fig. 17 that integrating FCLs in series to the DGs makes the fault current signals very close to its shape before connecting DGs in the distribution system. This manifests why the protection miscoordination is mitigated by FCLs. However, some miscoordinated devices can exist because static models of components are used to determine the FCL sizes in the second column of Table 7 by [12]. So, the above-obtained FCL size cannot be adequate to restore full coordination of devices considering the fault current transients and the HSFCL dynamics. As observed in Table 6, 12 miscoordination cases still exist for the SGWDSL scenario. The residual partial loss of protection coordination is due to ignoring the HSFCL dynamic behavior leading to inadequate sizing of the FCL resistance.

To consider the HSFCL dynamics, the proposed FCL sizing method in Section IV is used. Third column of Table 7 presents the obtained updated HSFCL resistance values that assure full coordination of protective devices considering dynamic models of all components. With the updated FCL sizes in Table 7, scenario SGWDDL is assessed in Table 6. It is noted that, for SGWDDL scenario, coordinated operation is verified for all main-backup pairs due to the corrected sizing of FCLs. According to Table 7, involving the dynamic

TABLE 6. Operating time difference between protection devices with different scenarios For IEEE 30 bus system.

main-backup devices	operating time difference, s					
	NGND	NGWD	IGWD	SGWD	SGWDSL	SGWDDL
R23BR1	-0.04	0.2	0.19	-0.09	0.21	0.31
R19BR1	0.21	0.24	0.37	-0.46	0.21	0.42
R23BR2	0.24	0.47	0.46	0.12	0.41	0.51
R15BR2	0.16	0.2	0.2	0.01	0.26	0.31
R23BR3	0.48	0.7	0.68	0.33	0.66	0.65
R15BR3	0.34	0.43	0.43	0.22	0.33	0.44
R19BR3	0.51	0.74	0.86	-0.04	-0.03	0.78
R19BR4	0.58	0.68	0.81	-0.09	0.25	0.71
R15BR4	0.34	0.38	0.38	0.17	0.4	0.41
R23BR4	0.35	0.64	0.63	0.29	0.52	0.41
R9BR5	-1.05	0.72	9.99	0.07	0.25	0.81
R12BR5	0.58	0.66	0.66	0.25	0.51	0.87
R8BR6	0.32	0.38	0.39	-0.18	0.01	0.41
R12BR6	0.06	0.2	0.21	-0.11	0.26	0.21
R8BR7	0.05	0.21	0.32	-0.51	0.2	0.22
R9BR7	0.09	9.38	9.38	-1.49	4.26	4.87
R6BR8	0.75	0.91	0.9	0.76	0.55	0.71
R16BR8	0.4	0.59	0.6	0.14	0.3	0.58
R5BR9	0.75	0.82	0.82	0.66	0.71	0.42
R16BR9	0.54	0.35	0.36	0.06	0.16	0.41
R5BR10	0.61	0.72	0.72	0.45	0.2	0.74
R6BR10	0.18	0.2	0.2	0.18	0.22	0.2
R5BR11	0.18	0.2	0.2	0.17	0.3	0.21
R6BR11	0.67	0.63	-9.19	0.86	0.59	0.63
R16BR11	0.17	0.2	-0.25	-0.19	0.18	0.25
R14BR12	0.29	0.3	0.3	0.31	0.26	0.34
R7BR13	0.17	0.2	0.2	0.16	0.23	0.31
R1BR14	0.19	0.2	0.2	0.16	0.25	0.54
R13BR15	0.62	0.8	0.8	0.74	1.15	0.81
R18BR16	0.34	0.24	0.24	0.23	2.99	0.24
R10BR17	0.15	0.2	0.2	0.18	0.13	0.27
R2BR18	0.2	0.22	0.21	0.26	0.41	0.22
R17BR19	0.12	0.2	0.22	0.28	0.33	0.28
R4BR20	0.25	0.29	0.3	0.29	0.03	0.24
R23BR20	0.04	0.29	0.29	0.25	0.03	0.35
R3BR21	0.19	0.21	0.21	0.15	-0.13	0.27
R4BR21	0.57	0.58	0.58	0.36	0.88	0.58
R23BR21	0.41	0.58	0.58	0.41	0.42	0.41
R4BR22	0.78	0.82	0.82	0.53	0.7	0.97
R25BR22	0.52	0.63	0.63	0.47	0.26	1.11
R11BR23	0.42	0.62	0.62	0.38	0.31	0.67
R25BR23	0.39	0.43	0.43	0.27	-0.82	0.24
R4BR24	0.16	0.2	0.2	-0.01	0.25	0.21
R11BR24	0.18	0.2	0.2	0.05	0.32	0.2
R24BR25	0.74	0.54	0.55	0.32	0.72	0.54
R29BR25	0.14	0.33	-5.12	-6.71	0.35	0.37
R24BR26	0.35	0.33	0.33	0.15	0.2	0.33
R24BR27	0.32	0.34	0.34	0.16	0.74	0.34
R26BR28	1.01	1.45	1.46	1.34	1	1.47
R27BR28	1.58	2.16	2.17	1.95	0.51	2.17
R27BR29	0.05	0.45	-0.77	-0.43	0.74	0.24
R7BRc16	0.34	0.6	0.6	0.5	1.03	0.64
R14BRc16	0.78	0.78	0.78	0.65	1.54	0.94
F1BF2	0.92	0.84	0.93	0.83	0.81	0.71
F1BRc16fm	0.42	0.53	0.53	0.23	0.71	0.52
F2BRc16fm	0.51	0.51	0.51	0.21	0.5	0.51
Rc16smBF1	0.42	0.5	0.5	0.15	0.51	0.57
Rc16smBF2	0.71	0.28	0.22	0.62	0.51	0.27
Rc16smBRc16fm	0.15	0.91	0.91	1.01	0.26	0.92
R13BRc17	0.89	0.9	0.9	0.8	0.33	0.9
R1BRc17	0.43	0.54	0.55	0.59	0.73	0.54

TABLE 6. *(Continued.)* **Operating time difference between protection devices with different scenarios For IEEE 30 bus system.**

F3BF4	1.22	1.25	1.25	1.19	2.05	1.25
Rc17smBF3	1.91	1.96	1.96	1.81	1.54	1.01
Rc17smBF4	0.26	0.26	0.26	0	0.25	0.26
F3BRc17fm	0.24	0.25	0.25	-0.01	0.25	0.27
F4BRc17fm	0.25	0.25	0.25	0.21	0.26	0.27
Rc17smBRc17fm	0.87	0.56	0.66	0.21	0.88	0.54
R27BRc30	0.24	0.65	0.55	0.19	0.35	0.65
R26BRc30	0.51	0.75	0.66	0.19	0.88	0.85
F5BF6	0.61	0.6	0.19	0.88	0.88	0.61
Rc30smBF5	0.54	0.25	0.37	0.35	0.35	0.27
Rc30smBF6	0.41	0.47	0.46	0.12	0.88	0.41
F5BRc30fm	0.87	0.26	0.26	0.27	0.54	0.26
F6BRc17fm	0.65	0.5	0.5	0.15	0.45	0.37
Rc30smBRc30fm	0.66	0.91	0.91	1.01	0.74	0.56
No. of miscoordinations	24	0	7	38	12	0

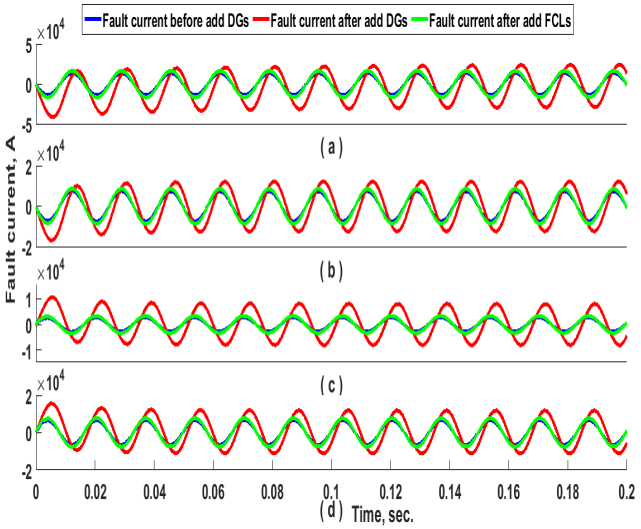

FIGURE 17. Examples of fault current signals before DGs, after DGs, and after static FCLs (a) Relay 5, (b) Relay 14, (c) Relay 16, (d) Relay 21.

TABLE 7. Location and sizes of FCLs for IEEE 30 bus system.

Location	Resistance, p.u	
	Neglecting all dynamics	Considering all dynamics
DG at Bus 10	5.42	6.91
DG at Bus 12	5.71	7.81
DG at Bus 19	4.41	8.51
Summation of FCLs sizes	15.54	23.23
Total FCLs cost	3.5M$	4.65 M$

behavior of FCLs caused an increase in the FCL size by about 50% and in the FCL cost by about 30%.

In the proposed method, the optimal settings and hence coordination between protective devices is maintained for a given arrangement of DGs, in terms of locations and sizes, by connecting an optimally-sized FCL in series to each DG unit to keep the fault current levels seen by the protective devices as close as possible to their levels before integration of DGs. The problem of protection miscoordination is more prominent with synchronous machine-based DG than inverter-based DG. In a previous work by the authors [1], it is shown that increasing the DG size, hence its fault current injection, up to twice the existing level does not deteriorate the protection coordination for the same FCLs. However, higher increase than 200% in the DG size can require enlarging the size of the associated FCL to sustain protection coordination. Furthermore, adding a new DG unit at the same node of a present one or at another node requires that a properly-sized FCL is inserted in series to the new DG to keep protection coordination intact without any need to tedious and risky devices re-setting especially for wide-area network [12]. This also will save the need for complicated and costly adaptive setting mechanisms for protective devices.

VII. CONCLUSION

A two-layer protection system is designed for a distribution network with distributed generators (DGs). The first layer comprises DOCRs to protect main feeders. The second includes autoreclosers and fuses to protect lateral feeders. IEEE 33-bus and modified 30-bus test systems are analyzed with the proposed protection scheme. Optimal settings of devices are determined to attain relay-relay, autorecloser-fuse, relay-autorecloser, and fuse-fuse coordination by constrained nonlinear optimization. Transient data of fault current and dynamic models of every protective device are considered. Current signals of both near-end and far-end faults are examined in the optimal setting problem to assure robust coordination. Besides, synchronous generator-based and inverter-based DGs are integrated to the distribution network. So, the fault current characteristics change causing loss of coordination between many pairs of protective devices. To keep coordination between all protective devices pairs under DGs, a hybrid superconducting fault current limiter (HSFCL) with high temperature superconducting resistive element is connected in series to each DG. HSFCL effectively reduces the fault current contribution of a DG. This makes the fault current seen by the protective device very similar to that current before integration of DGs. Therefore, coordination between protective devices is maintained in presence of DGs. An algorithm is proposed to minimize the cost of needed HSFCLs considering the dynamic models of HSFCL and the fault current transients. Multi-objective particle swarm optimization (MOPSO) is employed to specify the optimal HSFCLs sizes. Results show that considering the actual dynamic characteristics of system components causes about 30% increase in cost of HSFCLs compared to the conventional simplified sizing method to accomplish a robust and sustained coordination of protective devices. Application of the method in highly unbalanced distribution system can be a matter for future research. Also, comparative evaluation of the implications of different FCL types on the proposed method is a topic for future work.

REFERENCES

[1] A. Elmitwally, E. Gouda, and S. Eladawy, "Restoring recloser-fuse coordination by optimal fault current limiters planning in DG-integrated distribution systems," *Int. J. Electr. Power Energy Syst.*, vol. 77, pp. 9–18, May 2016.

[2] D. Saha, A. Datta, and P. Das, "Optimal coordination of directional overcurrent relays in power systems using symbiotic organism search optimisation technique," *IET Gener., Transmiss. Distrib.*, vol. 10, no. 11, pp. 2681–2688, 2016.

[3] S. M. Alaraifi and M. S. E. Moursi, "Hybrid HTS-FCL configuration with adaptive voltage compensation capability," *IEEE Trans. Appl. Supercond.*, vol. 24, no. 6, pp. 1–8, Dec. 2014.

[4] M. Ezzeddine and R. Kaczmarek, "A novel method for optimal coordination of directional overcurrent relays considering their available discrete settings and several operation characteristics," *Electr. Power Syst. Res.*, vol. 81, no. 7, pp. 1475–1481, Jul. 2011.

[5] M. M. Aly, H. Mahrous, and M. M. A. Mahmoud, "Recloser-fuse coordination of radial distribution systems with different technologies of distributed generation," in *Proc. Int. Conf. Innov. Trends Comput. Eng. (ITCE)*, Aswan, Egypt, Feb. 2019, pp. 420–425.

[6] M. A. Dawoud, D. K. Ibrahim, and M. Gilany, "Restoring recloser-fuse coordination in radial distribution networks with distributed generation," in *Proc. 19th Int. Middle East Power Syst. Conf. (MEPCON)*, Cairo, Egypt, Dec. 2017, pp. 170–175.

[7] M. N. Alam, B. Das, and V. Pant, "Protection scheme for reconfigurable radial distribution networks in presence of distributed generation," *Electr. Power Syst. Res.*, vol. 192, Mar. 2021, Art. no. 106973.

[8] S. Jamali and H. Borhani-Bahabadi, "Recloser time–current–voltage characteristic for fuse saving in distribution networks with DG," *IET Gener., Transmiss. Distrib.*, vol. 11, no. 1, pp. 272–279, Jan. 2017.

[9] K. Wheeler, M. Elsamahy, and S. Faried, "Use of superconducting fault current limiters for mitigation of distributed generation influences in radial distribution network fuse–recloser protection systems," *IET Gener., Transmiss. Distrib.*, vol. 11, no. 7, pp. 1605–1612, May 2017.

[10] U. Sultana, A. B. Khairuddin, M. M. Aman, A. S. Mokhtar, and N. Zareen, "A review of optimum DG placement based on minimization of power losses and voltage stability enhancement of distribution system," *Renew. Sustain. Energy Rev.*, vol. 63, pp. 363–378, Sep. 2016.

[11] P. Prakash and D. K. Khatod, "Optimal sizing and siting techniques for distributed generation in distribution systems: A review," *Renew. Sustain. Energy Rev.*, vol. 57, pp. 111–130, May 2016.

[12] A. Elmitwally, M. S. Kandil, E. Gouda, and A. Amer, "Mitigation of DGs impact on variable-topology meshed network protection system by optimal fault current limiters considering overcurrent relay coordination," *Electr. Power Syst. Res.*, vol. 186, Sep. 2020, Art. no. 106417.

[13] S. Ghobadpour, M. Gandomkar, and J. Nikoukar, "Determining optimal size of superconducting fault current limiters to achieve protection coordination of fuse-recloser in radial distribution networks with synchronous DGs," *Electr. Power Syst. Res.*, vol. 185, Aug. 2020, Art. no. 106357.

[14] A. Arafa, M. M. Aly, and S. Kamel, "Recloser-fuse coordination in radial distribution systems connected with distributed generation using saturated-core superconducting fault current limiter," in *Proc. Int. Conf. Innov. Trends Commun. Comput. Eng. (ITCE)*, Feb. 2020, pp. 385–390.

[15] R. S. F. Ferraz, A. C. Rueda-Medina, and O. E. Batista, "Genetic optimisation-based distributed energy resource allocation and recloser-fuse coordination," *IET Gener., Transmiss. Distrib.*, vol. 14, no. 20, pp. 4501–4508, Oct. 2020.

[16] N. Bayati, H. R. Baghaee, A. Hajizadeh, and M. Soltani, "A fuse saving scheme for DC microgrids with high penetration of renewable energy resources," *IEEE Access*, vol. 8, pp. 137407–137417, 2020.

[17] A. Safaei, M. Zolfaghari, M. Gilvanejad, and G. B. Gharehpetian, "A survey on fault current limiters: Development and technical aspects," *Int. J. Electr. Power Energy Syst.*, vol. 118, Jun. 2020, Art. no. 105729.

[18] A. Heidary, H. Radmanesh, K. Rouzbehi, A. Mehrizi-Sani, and G. B. Gharehpetian, "Inductive fault current limiters: A review," *Electr. Power Syst. Res.*, vol. 187, Oct. 2020, Art. no. 106499.

[19] A. Y. Hatata, A. S. Ebeid, and M. M. El-Saadawi, "Application of resistive super conductor fault current limiter for protection of grid-connected DGs," *Alexandria Eng. J.*, vol. 57, no. 4, pp. 4229–4241, Dec. 2018.

[20] R. M. Chabanloo, M. G. Maleki, S. M. M. Agah, and E. M. Habashi, "Comprehensive coordination of radial distribution network protection in the presence of synchronous distributed generation using fault current limiter," *Int. J. Electr. Power Energy Syst.*, vol. 99, pp. 214–224, Jul. 2018.

[21] T. Amraee, "Coordination of directional overcurrent relays using seeker algorithm," *IEEE Trans. Power Del.*, vol. 27, no. 3, pp. 1415–1422, Jul. 2012.

[22] F. A. Albasri, A. R. Alroomi, and J. H. Talaq, "Optimal coordination of directional overcurrent relays using biogeography-based optimization algorithms," *IEEE Trans. Power Del.*, vol. 30, no. 4, pp. 1810–1820, Aug. 2015.

[23] W. Rebizant, K. Solak, B. Brusilowicz, G. Benysek, A. Kempski, and J. Rusiński, "Coordination of overcurrent protection relays in networks with superconducting fault current limiters," *Int. J. Electr. Power Energy Syst.*, vol. 95, pp. 307–314, Feb. 2018.

[24] R. M. Chabanloo, H. A. Abyaneh, A. Agheli, and H. Rastegar, "Overcurrent relays coordination considering transient behaviour of fault current limiter and distributed generation in distribution power network," *IET Gener., Transmiss. Distrib.*, vol. 5, no. 9, pp. 903–911, 2011.

[25] R. M. Chabanloo and N. Mohammadzadeh, "A fast numerical method for optimal coordination of overcurrent relays in the presence of transient fault current," *IET Gener., Transmiss. Distrib.*, vol. 12, no. 2, pp. 472–481, Jan. 2018.

[26] A. S. Noghabi, J. Sadeh, and H. R. Mashhadi, "Considering different network topologies in optimal overcurrent relay coordination using a hybrid GA," *IEEE Trans. Power Del.*, vol. 24, no. 4, pp. 1857–1863, Oct. 2009.

[27] P. Yu, B. Venkatesh, A. Yazdani, and B. N. Singh, "Optimal location and sizing of fault current limiters in mesh networks using iterative mixed integer nonlinear programming," *IEEE Trans. Power Syst.*, vol. 31, no. 6, pp. 4776–4783, Nov. 2016.

[28] M. N. Alam, B. Das, and V. Pant, "Optimum recloser–fuse coordination for radial distribution systems in the presence of multiple distributed generations," *IET Gener., Transmiss. Distrib.*, vol. 12, no. 11, pp. 2585–2594, Jun. 2018.

[29] G. Benmouyal, M. Meisinger, J. Burnworth, W. A. Elmore, K. Freirich, P. A. Kotos, P. R. Leblanc, P. J. Lerley, J. E. McConnell, J. Mizener, J. P. de Sa, R. Ramaswami, M. S. Sachdev, W. M. Strang, J. E. Waldron, S. Watansiriroch, and S. E. Zocholl, "IEEE standard inverse-time characteristic equations for overcurrent relays," *IEEE Trans. Power Del.*, vol. 14, no. 3, pp. 868–872, Jul. 1999.

[30] M. R. Barzegar-Bafrooei and A. Akbari Foroud, "Performance evaluation of distance relay in the presence of hybrid SFCL," *IET Sci., Meas. Technol.*, vol. 12, no. 5, pp. 581–593, Aug. 2018.

[31] A. Arafa, M. M. Aly, and S. Kamel, "Impact of distributed generation on recloser-fuse coordination of radial distribution networks," in *Proc. Int. Conf. Innov. Trends Comput. Eng. (ITCE)*, Aswan, Egypt, Feb. 2019, pp. 505–509.

[32] R. Christie, "Power systems test case archive," Dept. Electr. Eng., Univ. Washington, Seattle, WA, USA, Tech. Rep. 1a998059, 2006. [Online]. Available: https://www2.ee.washington.edu/research/pstca

[33] Y. Valle, G. K. Venayagamoorthy, S. Mohagheghi, J. C. Hernandez, and R. G. Harley, "Particle swarm optimization: Basic concepts, variants and applications in power systems," *IEEE Trans. Evol. Comput.*, vol. 12, no. 2, pp. 171–195, Apr. 2008.

[34] M. M. Mansouri, M. Nayeripour, and M. Negnevitsky, "Internal electrical protection of wind turbine with doubly fed induction generator," *Renew. Sustain. Energy Rev.*, vol. 55, pp. 840–855, Mar. 2016.

[35] S. K. De and P. Raja, "A study on relay coordination in a distribution system with distributed generation and hybrid SFCL," in *Proc. IEEE Africon*, Pointe aux Piments, Mauritius, Sep. 2013, pp. 1–6.

[36] M. Reyes-Sierra and C. A. Coello, "Multi-objective particle swarm optimizers: A survey of the state-of-the-art," *Int. J. Comput. Intell. Res.*, vol. 2, no. 3, pp. 287–308, 2006.

[37] M. Rizwan, L. Hong, M. Waseem, S. Ahmad, M. Sharaf, and M. Shafiq, "A robust adaptive overcurrent relay coordination scheme for wind-farm-Integrated power systems based on forecasting the wind dynamics for smart energy systems," *Appl. Sci.*, vol. 10, no. 18, p. 6318, Sep. 2020.

EID ABDELBAKI GOUDA was born in Damietta, Egypt, in 1975. He received the B.Sc. and M.Sc. degrees in electrical engineering from Mansoura University, in 1997 and 2004, respectively, and the Ph.D. degree from the Groupe de Recherche en Electrotechnique et Electronique de Nancy, University Henri Poincare of Nancy, France, in 2011. He is currently an Associate Professor with the Electrical Department, Faculty of Engineering, Mansoura University. His research interests include magnetic gear, electric machine design/control and protection systems, renewable energy, power system analysis, and AI applications in power systems.

ADEL AMER received the B.S. degree in electrical engineering from Mansoura University, Egypt, in 2012. He is currently working as the Shift Leader in full O&M services at Siemens Energy. His research interests include power system operation and planning of hybrid renewable energy systems.

AKRAM ELMITWALLY (Member, IEEE) was born in Dakahlia, Egypt, in 1967. He received the B.Sc., M.Sc., and Ph.D. degrees from Mansoura University, Egypt, in 1989, 1995, and 2002, respectively, all in electrical power engineering. He was a Visiting Researcher with the Department of Electronic and Electrical Engineering, University of Bath, U.K., from 1998 to 2000. He is currently a Professor and the Head of the Department of Electrical Engineering, Mansoura University. He has authored more than 80 papers in journals and conferences. His research interests include power quality, power system protection, dispersed generation, and AI applications in energy systems. He is a registered engineer in Egypt. He is a reviewer and an editorial board member of a number of specialized international journals.